CL-170423 Received: April 24, 2017 | Accepted: May 28, 2017 | Web Released: June 3, 2017

Polarization-dependent Total Reflection Fluorescence X-ray Absorption Fine Structure (PTRF-XAFS) Studies on the Structure of a Pt Monolayer on Au(111) Prepared by the Surface-limited Redox Replacement Reaction

Qiuyi Yuan,[1] Satoru Takakusagi,[1] Yuki Wakisaka,[1] Yohei Uemura,[2] Takahiro Wada,[3] Hiroko Ariga,[1] and Kiyotaka Asakura*[1]
[1]*ICAT, Hokkaido University, Kita 21 Nishi 10, Kita-ku, Sapporo, Hokkaido 001-0021*
[2]*Institute for Molecular Science, Okazaki, Aichi 444-0867*
[3]*Tokyo Medical and Dental University, Tokyo 113-8510*

(E-mail: askr@cat.hokudai.ac.jp)

We studied the initial stage of a Pt monolayer produced by surface-limited redox replacement (SLRR) using polarization-dependent total reflection fluorescence X-ray absorption fine structure (PTRF-XAFS). Different from the widely accepted understanding that metallic monolayer islands are formed, our XAFS showed that the Pt monolayer, initially present on the Au(111) substrate, was mainly in the form of a planar $[PtCl_4]^{2-}$ complex with its molecular plane parallel to Au(111). This result provides a new insight into the mechanism of SLRR.

Keywords: X-ray absorption fine structure (XAFS) | Surface-limited redox replacement reaction | Pt monolayer

Polymer electrolyte fuel cells (PEFCs), which emit no greenhouse gases, have attracted much attention because of the necessity for the modern society to shift from fossil fuels to clean energy. However, several issues concerning electrocatalysts, including their cost and durability, have greatly inhibited the practical use of PEFCs.[1] To reduce the cost of the electrocatalyst, we need to increase the surface area of Pt, which is the main component of the fuel cell catalyst currently. Considerable effort has been devoted to investigating the electrodeposition of Pt.[2–4] Owing to the high surface energy and low wettability of Pt, it is difficult to obtain monolayer deposition on a flat surface with conventional electrodeposition methods.[2,4] Brankovic et al. developed a method for Pt monolayer deposition by galvanic displacement of a layer of sacrificial underpotential deposition (UPD) metal, which is called surface-limited redox replacement (SLRR).[5] Several sacrificial materials, like Cu,[6–8] Pb,[7,9] and H,[10] have been studied for the deposition of Pt monolayers. In addition to Pt, the SLRR was extended to the monolayer deposition of other metals, such as Pd,[11] Ru,[12] and Ag.[5,13] Furthermore, bimetallic monolayer depositions were also achieved by the SLRR.[14,15] However, there are only limited numbers of studies regarding the mechanism of the deposition process on atomic levels. In situ scanning tunneling microscopy (STM) was used to study the structure of Pt submonolayers.[8] Brankovic et al. systematically studied the reaction mechanism of SLRR to replace the UPD Cu with Pt. They proposed a kinetic model,[16] based on the stoichiometry of SLRR,[6] and also proposed the nucleation mechanism of the Pt monolayer clusters,[17] and the UPD procedure on the Pt monolayer modified surface.[9,15] However, some aspects remain unclear. For example, what is the chemical state and structure of the Pt submonolayers and Pt submonolayer–Au interaction, which are very important parameters since they are related to the catalytic properties? To examine the Pt initial structure created by the SLRR of the Cu UPD layer, we applied polarization-dependent total reflection fluorescence-X-ray absorption fine structure (PTRF-XAFS) techniques.[18–20] PTRF-XAFS is a powerful way of characterizing the surface structure and electronic state of less than a monolayer of adsorbate on atomically flat surfaces even under the electrochemical condition.[21–24] Although the coverage of Pt was only around 0.45 ML in our sample, according to previous STM results,[6] we could successfully measure the Pt L_3 edge XAFS. In addition, the polarization-dependent XAFS data revealed the 3-dimensional structure of the Pt species. In this work, we measured two polarizations of the Pt L_3 edge XAFS parallel (s-pol) and perpendicular (p-pol) to the surface. Surprisingly, we found that $[PtCl_4]^{2-}$ was the main species present on the Au surface at the initial stage, which was different from the model widely accepted in the SLRR process where Pt is completely reduced.

A Pt monolayer on Au(111) (denoted as Pt/Au(111) below) was synthesized following the protocol. An electrochemically polished and flame-annealed Ø10 mm Au(111) single crystal was used as the working electrode. The Au(111) surface was characterized by a cyclic voltammetry (CV) scan in 0.05 M H_2SO_4 (Figure S1a). The synthesis of Pt/Au(111) was conducted inside a glovebox filled with Ar. The Pt/Au(111) was prepared through SLRR of Cu UPD in Ar-deaerated solutions. A Cu monolayer was deposited at the UPD potential in 0.1 M $HClO_4$ + 1 mM $Cu(ClO_4)_2$ (CV shown in Figure S1b). Then, the Cu monolayer was displaced with Pt species in 0.1 M $HClO_4$ + 1 mM H_2PtCl_6 for 30 s. After the synthesis was completed, the sample was transferred to the in situ XAFS cell inside the glovebox. The cell was a homemade poly(chlorotrifluoroethylene) (PCTFE) cell,[25] with a 6 µm Mylar film as an X-ray window, as shown in Figure S3. In order to find out the potential for in situ XAFS, the Pt/Au(111) surface was characterized by a CV scan in 0.1 M $HClO_4$ as shown in Figure S2 for 10 cycles. The 1st scan showed a cathodic peak around 0.3 V, which was not reproducible in the subsequent scans. Therefore, the in situ XAFS potential was chosen at 0.45 V, which was before the cathodic peak onset and 0.05 V lower than the open circuit potential (OCP) at 0.5 V, without any other potential applied after the replacement reaction. All the potentials were denoted with respect to the Ag/AgCl reference electrode unless otherwise labeled (saturated KCl solution). Pt L_3 edge PTRF-XAFS measurements were performed at the BL12C beamline in the Photon Factory, Institute for Materials Structure Science, High Energy Accelerator Research Organization (PF-IMSS-KEK). X-rays were monochromatized with a Si(111) double crystal monochromator and the fluorescence

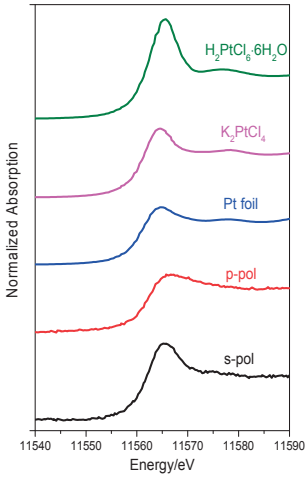

Figure 1. XANES comparison between the Pt/Au(111) at $E = 0.45$ V (s- and p-polarization) with a standard reference Pt foil and Pt complexes (K_2PtCl_4 and $H_2PtCl_6 \cdot 6H_2O$).

signal was detected by a 19-element Ge solid state detector (MSSD; Canberra). Higher harmonics were rejected by the focusing mirror. The in situ XAFS cell was mounted on a five-axis goniometer to allow the fine adjustment for the total reflection conditions and polarization directions (Figure S4). A Zn filter ($\mu t = 3$) was placed in front of the MSSD to reduce the elastic scattering from the substrate. The XAFS analysis was carried out using the software REX2000.[26–28] FEFF8 was used for XAFS simulations.[29,30] The degree of the agreement in the simulations was estimated by $|R|^2$ using the following equation:

$$|R|^2 = \frac{1}{N_{\mathrm{dat}}} \sum_i \frac{(\chi_i^{\mathrm{data}}(k) - \chi_i^{\mathrm{fit}}(k))^2}{\varepsilon_i^2} \quad (1)$$

Here, χ_i^{data} and χ_i^{fit} are the experimental and fitted EXAFS oscillations, respectively. N_{dat} is the number of data points used in fitting. ε_i is the standard deviation at each data point. When R is less than 1, the model fitting is acceptable.

Figure 1 shows the normalized L_3 edge X-ray absorption near-edge structure (XANES) of the Pt monolayer with comparison to the reference samples. The L_3 edge white line (WL) intensity is directly related to the amount of unfilled d states.[31] Although the WL peak of the p-polarization at 0.45 V is a little broader than that of the Pt foil, the intensity of s-polarization at 0.45 V is stronger than that of the reference $[PtCl_4]^{2-}$ but weaker than that of $[PtCl_6]^{2-}$, showing that the Pt monolayer was not fully reduced to Pt^0. Additionally, the WL intensity of p-polarization was much lower than that of the s-polarization. We will discuss this in more detail at a later stage.

Figure 2 shows the extended X-ray absorption fine structure (EXAFS) spectra of Pt on Au(111) for s- and p-polarization. The EXAFS spectra were cut at $k = 8$ Å^{-1} owing to the close absorption edge of the Au substrate. The oscillation periods of s- and p-polarization EXAFS spectra were almost the same though the EXAFS amplitude of s-polarization was nearly twice as large as that of the p-polarization. To derive the detailed structure information, FEFF8 simulation was performed. We postulated the following model structures: (a) Pt metal monolayer having a commensurate structure with an Au surface, (b) PtO_2 monolayer, and (c) $PtCl_x^{y-}$.

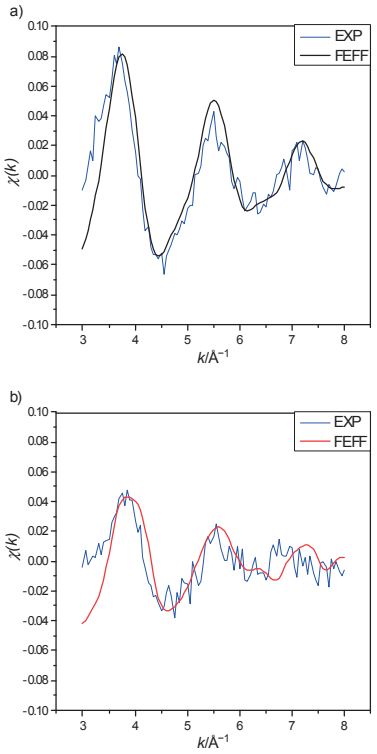

Figure 2. EXAFS comparison between the experimental data and FEFF calculation for the Pt/Au(111) at $E = 0.45$ V. a) s-Polarization and b) p-polarization.

The Pt commensurate monolayer was rejected as shown in Figures S5a and S5b. Since the Pt–Pt distance in the s-polarization was 0.288 nm in the commensurate structure, the oscillation period did not follow the observed period. One had to reduce the Pt–Pt distance to 0.254 nm to follow the experimental oscillation, which was very short compared with the normal Pt–Pt distance. In addition, we could not reproduce the EXAFS oscillation only by the Pt–Pt interaction even if the Pt–Pt distance was contracted to 0.254 nm. Thus, it was difficult to state that the Pt metallic monolayer was fully formed by the SLRR. The Pt oxides with Pt–O distance of 0.203 nm[32] were also ruled out as shown in Figures S5c and S5d.

Finally, Pt–Cl complexes were tested and we obtained good fitting results. Preliminary curve fitting indicated the presence of Pt–Cl at approximately 0.23 nm. This suggested that the Pt species on Au were mainly Pt–Cl complexes. We further simulated the EXAFS oscillations with several Pt–Cl models adsorbed on different sites of Au(111). Figure 3 shows the best fitted model, where a square planar $[PtCl_4]$ complex was adsorbed on Au(111) at a top site. Pt was surrounded with Cl at 0.226 nm. The $[PtCl_4]$ plane was parallel to the surface on top of the Au with the Pt–Au distance being 0.270 nm. The R factors for both s- and p-polarization spectra were 0.46 and 0.58, respectively, meaning that the model should not be rejected.

One may ask why Pt–Cl was found in a p-polarization even though the polarization was perpendicular to the Pt–Cl bond. This arose from the imperfect polarization dependence of the L_3 edge EXAFS:[33]

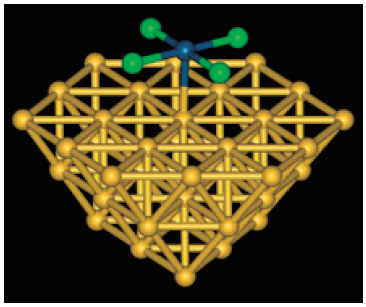

Figure 3. A $PtCl_4$ complex model on Au(111) used in the FEFF simulation. Yellow, green, and blue balls are Au, Cl, and Pt atoms, respectively. The Pt–Cl complex preserved the square planar $[PtCl_4]^{2-}$ structure with Pt on top of the Au atom. The Pt–Cl bond length is 0.226 nm for all four bonds, while the Pt–Au distance is 0.270 nm.

$$\chi^*(k,\Theta) = \frac{1}{2}\sum_{i=1}^{N}(1.2 + 2.4\cos^2\theta_i)\chi_i(k) \qquad (2)$$

where $\chi^*(k,\Theta)$ and $\chi_i(k)$ are the total and partial EXAFS oscillation accompanied with the i-th bond, respectively. θ_i is the angle between the X-ray electric field direction $\hat{\mathbf{e}}$ and the i-th bonding direction, $\boldsymbol{r}_i$. Θ is the angle between electric field direction and surface normal vector. In addition to the cosine-square-polarization-dependent term, the equation also contains an isotropic term. When the model of $[PtCl_4]$ with a square planar plane parallel to the Au(111) surface was assumed, the effective coordination number from eq 2 would be 4.8 and 2.4 for s- and p-polarization, respectively, which fitted well with the observed data. The Pt–Cl bond length given by the model was 0.226 nm, which was shorter than that of the reference K_2PtCl_4, which had a Pt–Cl distance at 0.232 nm. The Debye–Waller factor of the Pt–Cl bond was 0.0084 nm and the energy shift was −7 eV.

Another important question regarding the model was whether a direct Pt–Au bonding was present between $[PtCl_4]^{2-}$ and the Au surface. A discussion is included in the SI, where we separated the Pt–Au oscillation from the s- and p-polarization spectra as shown in Figure S6. However, there is still a lack of sufficient evidence to reach the conclusion that there is a Pt–Au bond formed based on our current data.

Based on this structure, we interpreted the XANES shape and its polarization dependence. We noticed that in XANES, the WL intensity of s-polarization was much higher than that of p-polarization. Based on our model, if the Pt–Cl complex had the square planar structure of $[PtCl_4]^{2-}$ (or d^8 complex), the $d_{x^2-y^2}$ of d-orbitals, directed by the ligands, were split as shown in Figure S7. The $d_{x^2-y^2}$ had the highest energy and was not filled. The other orbitals, d_{xy}, d_{yz}, d_{xz}, and d_{z^2} should all be filled in the square planar complex. Therefore, only the transition to the $d_{x^2-y^2}$ from p states was allowed. For the s-polarization, the p_x and p_y orbitals were excited while the p_z orbital was not allowed in the p-polarization, so that the s-polarization provided a larger WL. If the structure was $[PtCl_4]^{2-}$ as we proposed, we could average the polarization-dependent XANES using the following equation:

$$\mu_{\text{unpol}} = (2\mu_s + \mu_p)/3 \qquad (3)$$

The integrated unpolarized spectrum based on the above equation is shown in Figure 4. The WL intensity was comparable with the

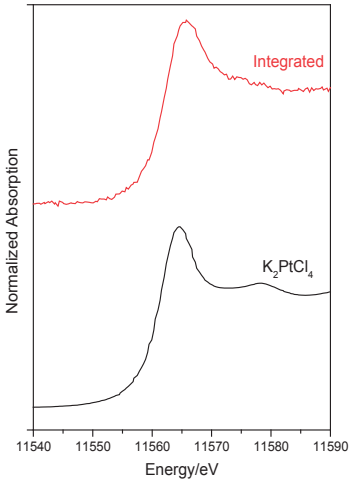

Figure 4. Comparison of the integrated XANES calculated based on eq 3 with the reference K_2PtCl_4 sample.

intensity of the unpolarized spectrum of 2.21 ± 0.26 eV and the reference sample K_2PtCl_4 of 2.20 ± 0.08 eV, though the shape was different with a broader shoulder, and a FWHM of 4.7 eV compared with 4.0 eV of the reference K_2PtCl_4. This arose from the broad and weak WL in the p-polarization spectrum as shown in Figure 1, which could indicate the presence of the Pt–Au interaction.

Unlike previous studies of Pt on the Au prepared by SLRR where a Pt metallic layer was present on Au[34–36] we found the Pt was mainly in the state of $[PtCl_4]^{2-}$. The potential applied during in situ XAFS was 0.45 V, which was lower than that for the formation of Pt–OH at 0.7 V and the redox potential of $[PtCl_4]^{2-}$/Pt and $[PtCl_6]^{2-}$/$[PtCl_4]^{2-}$ (0.56 and 0.53 V) under standard conditions. The OCP of Pt/Au in 0.1 M $HClO_4$ was around 0.5 V. The electrode potential applied here was lower than both OCP and the reduction of Pt–OH at around 0.55 V. Imperfect reduction of the Pt species and the stabilization of $[PtCl_4]^{2-}$ may arise from the strong interaction of $[PtCl_4]^{2-}$ and the substrate as suggested by Kolb.[2] Kolb et al. also found that the $(\sqrt{7}\times\sqrt{7})R19.1^\circ$ adlayer of $[PtCl_4]^{2-}$ was on the Au(111) at the potential between the oxidation of the substrate and the onset of Pt deposition.[2] As mentioned above, they suggested a strong interaction between $[PtCl_4]^{2-}$ and the Au surface, which may stabilize the $[PtCl_4]^{2-}$ species on Au. Our results revealed the possibility that the Pt monolayer just after SLRR might not be reduced to Pt metal but reduced to the $[PtCl_4]^{2-}$ complex from the original $[PtCl_6]^{2-}$. This phenomenon could assist us to explain the different kinetics of the displacement reactions.[37]

We found a new structure of Pt species, $[PtCl_4]^{2-}$, which was the main species in Pt/Au(111), using in situ PTRF-XAFS. This result provides new insight into the mechanism of SLRR and a different understanding of the behavior of the SLRR-derived Pt monolayer of its electrocatalytic properties. We are now analyzing the data to confirm the possibility for the presence of a minor Pt metallic state.

The authors would like to express their gratitude to the NEDO PMFC project for their financial support. We thank Dr. Y. Niwa, Dr. H. Nitani, Dr. H. Abe and Prof. M. Kimura at

the Photon Factory of the Institute for Materials Science, Tsukuba. The work was carried out under the approval of PAC (Proposal Nos. 2015G070, 2016G035). This work was supported by the Technical Division of Institute for Catalysis, Hokkaido University.

Supporting Information is available on http://dx.doi.org/10.1246/cl.170423.

References

1 M. K. Debe, *Nature* **2012**, *486*, 43.
2 H.-F. Waibel, M. Kleinert, L. A. Kibler, D. M. Kolb, *Electrochim. Acta* **2002**, *47*, 1461.
3 K. Uosaki, S. Ye, Y. Oda, T. Haba, K. Hamada, *Langmuir* **1997**, *13*, 594.
4 K. Uosaki, S. Ye, H. Naohara, Y. Oda, T. Haba, T. Kondo, *J. Phys. Chem. B* **1997**, *101*, 7566.
5 S. R. Brankovic, J. X. Wang, R. R. Adžić, *Surf. Sci.* **2001**, *474*, L173.
6 D. Gokcen, S.-E. Bae, S. R. Brankovic, *J. Electrochem. Soc.* **2010**, *157*, D582.
7 M. F. Mrozek, Y. Xie, M. J. Weaver, *Anal. Chem.* **2001**, *73*, 5953.
8 Y.-G. Kim, J. Y. Kim, D. Vairavapandian, J. L. Stickney, *J. Phys. Chem. B* **2006**, *110*, 17998.
9 Q. Yuan, A. Tripathi, M. Slavkovic, S. R. Brankovic, *Z. Phys. Chem.* **2012**, *226*, 965.
10 J. Nutariya, M. Fayette, N. Dimitrov, N. Vasiljevic, *Electrochim. Acta* **2013**, *112*, 813.
11 L. B. Sheridan, D. K. Gebregziabiher, J. L. Stickney, D. B. Robinson, *Langmuir* **2013**, *29*, 1592.
12 C. Thambidurai, Y.-G. Kim, J. L. Stickney, *Electrochim. Acta* **2008**, *53*, 6157.
13 R. Vasilic, L. T. Viyannalage, N. Dimitrov, *J. Electrochem. Soc.* **2006**, *153*, C648.
14 N. Jayaraju, D. Banga, C. Thambidurai, X. Liang, Y.-G. Kim, J. L. Stickney, *Langmuir* **2014**, *30*, 3254.
15 L. C. Grabow, Q. Yuan, H. A. Doan, S. R. Brankovic, *Surf. Sci.* **2015**, *640*, 50.
16 D. Gokcen, S.-E. Bae, S. R. Brankovic, *Electrochim. Acta* **2011**, *56*, 5545.
17 D. Gokcen, Q. Yuan, S. R. Brankovic, *J. Electrochem. Soc.* **2014**, *161*, D3051.
18 K. Asakura, *Catal. Today* **2010**, *157*, 2.
19 K. Asakura, in *Catalysis*, ed. by J. J. Spivey, M. Gupta, RSC Publishing, Cambrige, **2012**, Vol. 24, p. 281. doi:10.1039/9781849734776-00281.
20 K. Asakura, S. Takakusagi, H. Ariga, W.-J. Chun, S. Suzuki, Y. Koike, H. Uehara, K. Miyazaki, Y. Iwasawa, *Faraday Discuss.* **2013**, *162*, 165.
21 S. Takakusagi, W.-J. Chun, H. Uehara, K. Asakura, Y. Iwasawa, *Top. Catal.* **2013**, *56*, 1477.
22 H. Uehara, M. H. B. Hanaffi, Y. Koike, K. Fujikawa, S. Suzuki, H. Ariga, S. Takakusagi, W.-J. Chun, Y. Iwasawa, K. Asakura, *Chem. Phys. Lett.* **2013**, *570*, 64.
23 H. Uehara, Y. Uemura, T. Ogawa, K. Kono, R. Ueno, Y. Niwa, H. Nitani, H. Abe, S. Takakusagi, M. Nomura, Y. Iwasawa, K. Asakura, *Phys. Chem. Chem. Phys.* **2014**, *16*, 13748.
24 S. Takakusagi, A. Kunimoto, N. Sirisit, H. Uehara, T. Ohba, Y. Uemuara, T. Wada, H. Ariga, W.-J. Chun, Y. Iwasawa, K. Asakura, *J. Phys. Chem. C* **2016**, *120*, 15785.
25 T. Kondo, K. Tamura, M. Takahasi, J. Mizuki, K. Uosaki, *Electrochim. Acta* **2002**, *47*, 3075.
26 K. Asakura, in *X-ray Absorption Fine Structure for Catalyst and Surfaces*, ed. by Y. Iwasawa, World Scientific, Singapore, **1996**, Vol. 2, p. 33.
27 T. Taguchi, T. Ozawa, H. Yashiro, *Phys. Scr.* **2005**, 205.
28 T. Taguchi, *AIP Conf. Proc.* **2007**, *882*, 162.
29 J. J. Rehr, R. C. Albers, *Rev. Mod. Phys.* **2000**, *72*, 621.
30 A. L. Ankudinov, B. Ravel, J. J. Rehr, S. D. Conradson, *Phys. Rev. B* **1998**, *58*, 7565.
31 A. N. Mansour, J. W. Cook, Jr., D. E. Sayers, *J. Phys. Chem.* **1984**, *88*, 2330.
32 W. J. P. L. Moore, Jr., *J. Am. Chem. Soc.* **1941**, *63*, 3.
33 S. M. Heald, E. A. Stern, *Phys. Rev. B* **1977**, *16*, 5549.
34 M. B. Vukmirovic, J. Zhang, K. Sasaki, A. U. Nilekar, F. Uribe, M. Mavrikakis, R. R. Adzic, *Electrochim. Acta* **2007**, *52*, 2257.
35 J. Zhang, M. B. Vukmirovic, Y. Xu, M. Mavrikakis, R. R. Adzic, *Angew. Chem., Int. Ed.* **2005**, *44*, 2132.
36 A. U. Nilekar, M. Mavrikakis, *Surf. Sci.* **2008**, *602*, L89.
37 T. S. Mkwizu, I. Cukrowski, *Electrochim. Acta* **2014**, *147*, 432.

